J. Fluid Mech. (1989), *vol.* 208, *pp.* 639–656
Printed in Great Britain

Wave patterns in plane Poiseuille flow created by concentrated disturbances

By FEI LI AND SHEILA E. WIDNALL
Department of Aeronautics and Astronautics, Massachusetts Institute of Technology, Cambridge, MA 02139, USA

(Received 9 May 1987 and in revised form 13 February 1989)

A model is constructed for perturbations created in the surrounding laminar flow by a turbulent spot in plane Poiseuille flow. The turbulent spot is represented as a distribution of increased Reynolds stress, which travels steadily through the surrounding laminar flow. The Navier–Stokes equations are linearized and are solved by using Fourier transforms in the plane parallel to the channel walls and a finite-difference method in the direction perpendicular to the walls. The travelling Reynolds stress distribution acts as a forcing term in the equations.

Numerical results show that a packet of oblique waves are generated around the disturbance when the force is antisymmetric with respect to the channel centreline, whereas no identifiable wave crests are found when the forcing is symmetric. Furthermore, wavelengths of the typical waves composing the packet are insensitive to the size of the region of Reynolds stress. The dependencies of the flow field on Reynolds number and spot speed are investigated. In the case of symmetric forcing, the flow is forced around the disturbance, causing distortions to the basic velocity profiles. These results are in qualitative agreement with experimental observations.

1. Introduction

The laminar–turbulent transition process in a shear flow has been one of the most studied fluid dynamic phenomena since its discovery by Osborne Reynolds (1883) over a century ago. The fact that there are many routes by which a flow may undergo transition makes the investigation of the transition process especially difficult and challenging. Linear stability theory is successful in explaining the onset of transition for some flow situations (e.g. boundary-layer flow), but is unsatisfactory for others (e.g. plane Poiseuille flow).

Linear waves first become unstable when the Reynolds number exceeds a critical value. An accurate value for the critical Reynolds number for linear disturbances in plane Poiseuille flow was foundby Orszag (1971) to be 5772. The experiment of Nishioka, Iida & Ichikawa (1975) showed that under very carefully controlled conditions, linear waves become unstable at a Reynolds number of about 6000. Stuart (1960) showed that waves become unstable when their amplitudes exceed a threshold at Reynolds numbers greater than about 2800. However, transition to turbulence in plane Poiseuille flow has been observed to occur much earlier than predicted by either linear or nonlinear theory. In fact, a turbulent spot in plane Poiseuille flow can be generated and grow at $Re = 1000$ as was shown by the experiment of Carlson, Widnall & Peeters (1982). Orszag & Kells (1978) numerically solved the Navier–Stokes equations and found that three-dimensional finite-amplitude disturbances are destabilizing and can drive transition to turbulence at a

Reynolds number of about 1000. Orszag & Patera (1980, 1981, 1983) analysed subcritical transition to turbulence and showed that two-dimensional finite-amplitude waves were exponentially unstable to three-dimensional linear secondary waves.

In addition to the investigations focused on the secondary instability of two-dimensional waves, research on the response of a shear flow to localized disturbances has also been done.

Gaster & Grant (1975) experimentally investigated the formation and development of a wave packet in a laminar boundary layer created by a pulsed disturbance at a point on the boundary. Their experimental results were compared with the theoretical model of Gaster (1975) and good agreement was found. The wave packet resulting from a pulsed disturbance was modelled as a superposition of solutions to the Orr–Sommerfeld equation.

Carlson *et al.* (1982) presented a flow visualization study of the growth of turbulent spots in plane Poiseuille flow using a water channel of width-to-depth ratio of 133 and observed that both natural and artificially triggered turbulent spots could grow at Reynolds number as low as 1000. They obtained photographs of the turbulent spots showing oblique waves in the laminar flow surrounding the spot.

From the results of Gaster (1975) discussed above, one concludes that linear theory will predict that a disturbance in a shear flow will grow only at supercritical Reynolds numbers as given by linear theory so that such a calculation would offer little insight to the observed growth of turbulent spots in plane Poiseuille flow.

In exploring the findings of Carlson *et al.* (1982), Widnall (1984) raised the following questions. First, how is the turbulent spot able to grow in a stable viscous background where all linear and weakly nonlinear free waves decay? Second, how and why are the waves generated? Is there a preferred wavelength? Finally, what role do the waves play in the growth of the localized turbulence? Widnall proposed that the turbulent spot acts as a region of disturbance which generates waves in a manner similar to that of a ship moving on a free surface and forces the oblique waves to amplitudes such that they become unstable to three-dimensional secondary disturbances along their crests. These instabilities break down further into small-scale turbulence which increases the size of the region of disturbance and the cyclical process continues. A mathematical model was constructed which modelled the region of disturbance as a steady travelling delta-function, leading to a non-homogeneous Orr–Sommerfeld equation. Unlike the solution of a pulsed disturbance in a subcritical shear flow, which would decay downstream, a solution forced by a travelling disturbance will retain its form. A far-field solution was obtained using the method of stationary phase which showed qualitative agreement with the experiment of Carlson *et al.* (1982). In this paper we extend this approach to obtain a complete linear flow-field solution for such a forced disturbance.

Henningson & Alfredsson (1987) experimentally investigated the wave packets generated by the turbulent spot in plane Poiseuille flow by hot-film anemometry. They found that the steamwise velocity disturbance associated with the waves was antisymmetric with respect to the channel centreline, and showed that the wave packet consisted of the locally, least-stable Tollmien–Schlichting mode. A symmetric disturbance in the spanwise velocity was found directed towards the spot downstream of the spot, and away from the spot upstream, indicating a blockage effect, consistent with the idea of Widnall (1984). They also did a linear stability analysis of the modified velocity profiles measured in the experiment and found, by

considering the eigenvalues of the Orr–Sommerfeld equation, that the modified flow field was less stable than the undisturbed flow, although the amplification rates they computed are too small to explain the observed growth of the waves.

A flow visualization experiment of turbulent spots in plane Poiseuille flow was also done by Alavyoon, Henningson & Alfredsson (1986), and recently a full Navier–Stokes simulation was carried out by Henningson, Sparlart & Kim (1987). These experiments and calculations were in good agreement and determined the speed of advection, spreading half-angle of the spot and some properties of the wave field around the spot.

Although it is clear that the propagation and growth of a turbulent spot in plane Poiseuille flow is inherently a nonlinear process, it is of some interest to determine whether some properties of the observed wave field can be related to the linear wave field generated in the laminar shear flow by a steady travelling disturbance. In this analysis, the small-scale turbulence in the spot is modelled as a region of increased Reynolds stress. Both symmetric and antisymmetric disturbances are considered. The focus of the investigation is the structure of the wave field and the effects of changing the flow parameters on the wave pattern. The numerical results show that the present formulation is of some value in describing certain features of the wave field generated by a concentrated disturbance. This investigation does not provide a complete analysis of the turbulent spot since subsequent secondary instabilities of the wave field and modifications to the mean velocity profile require a nonlinear analysis.

2. Formulation

We begin with the full incompressible unsteady Navier–Stokes equations and choose a coordinate system such that the x-axis is parallel to and in the direction of the unperturbed flow, the y-axis is parallel to the walls and perpendicular to the direction of the unperturbed flow, and the z-axis is perpendicular to the walls. The frame of reference is fixed to the turbulent spot, which travels with velocity, c_s.

$$\frac{\partial \boldsymbol{v}}{\partial t} + \boldsymbol{v}\cdot\boldsymbol{\nabla}\boldsymbol{v} = \frac{-1}{\rho}\boldsymbol{\nabla}p + \nu\nabla^2\boldsymbol{v}, \tag{1}$$

$$\boldsymbol{\nabla}\cdot\boldsymbol{v} = 0, \tag{2}$$

where $\boldsymbol{v}$ is the velocity vector, p is the pressure, ρ is the fluid density, ν is the kinematic viscosity. We non-dimensionalize the lengthscales by the channel half-depth h, the velocities by the maximum mean velocity in the channel U_0, pressure by the term ρU_0^2 and time by $h/U_0\theta$, where θ is a chosen non-dimensional quantity (to be defined later in this section) so that the non-dimensionalized derivative, $\partial\boldsymbol{v}/\partial t$, is of order 1. The non-dimensional equations are

$$\theta\frac{\partial \boldsymbol{v}}{\partial t} + \boldsymbol{v}\cdot\boldsymbol{\nabla}\boldsymbol{v} = -\boldsymbol{\nabla}p + \frac{1}{Re}\nabla^2\boldsymbol{v}, \tag{3}$$

$$\boldsymbol{\nabla}\cdot\boldsymbol{v} = 0, \tag{4}$$

where $Re = U_0 h/\nu$ is the Reynolds number, and all variables are understood as non-dimensional.

In the presence of a turbulent spot the flow field is perturbed from that of the

parallel laminar flow. We define the large-scale deviations of velocity vector, $\tilde{\boldsymbol{v}}$, and pressure, $\tilde{p}$, as follows:

$$\tilde{\boldsymbol{v}} = \overline{\boldsymbol{v} - U(z)\boldsymbol{i}}, \tag{5}$$

$$\tilde{p} = \overline{p - P}, \tag{6}$$

where the overbar indicates ensemble average, $U(z)$ and P are the velocity and pressure of the unperturbed laminar flow respectively and $\boldsymbol{i}$ is the unit vector in the x-direction. Hence, we can split the velocity vector and the pressure each into three components and derive the governing equation in the same manner as did Landahl (1975) in his two-scale model for wave breakdown and turbulence,

$$\boldsymbol{v} = U(z)\,\boldsymbol{i} + \tilde{\boldsymbol{v}} + \boldsymbol{v}', \tag{7}$$

$$p = P + \tilde{p} + p', \tag{8}$$

where $\boldsymbol{v}'$ and p' are turbulent fluctuations of velocity and pressure in the perturbed flow field whose ensemble averages are zero.

We now substitute (7) and (8) into (3) and (4), take the ensemble average and substract the equation of the unperturbed laminar flow

$$\frac{1}{Re}\frac{\mathrm{d}^2 U}{\mathrm{d}z_2} = \frac{\mathrm{d}P}{\mathrm{d}x} \tag{9}$$

to obtain the following equations:

$$\theta\frac{\partial u}{\partial t} + U\frac{\partial u}{\partial x} + w\frac{\mathrm{d}U}{\mathrm{d}z} = -\frac{\partial p}{\mathrm{d}x} + \frac{1}{Re}\nabla^2 u + \frac{\partial \tau_{xx}}{\partial x} + \frac{\partial \tau_{xy}}{\partial y} + \frac{\partial \tau_{xz}}{\partial z}, \tag{10}$$

$$\theta\frac{\partial v}{\partial t} + U\frac{\partial v}{\partial x} = -\frac{\partial p}{\partial y} + \frac{1}{Re}\nabla^2 v + \frac{\partial \tau_{yx}}{\partial x} + \frac{\partial \tau_{yy}}{\partial y} + \frac{\partial \tau_{yz}}{\partial z}, \tag{11}$$

$$\theta\frac{\partial w}{\partial t} + U\frac{\partial w}{\partial x} = -\frac{\partial p}{\partial z} + \frac{1}{Re}\nabla^2 w + \frac{\partial \tau_{zx}}{\partial x} + \frac{\partial \tau_{zy}}{\partial y} + \frac{\partial \tau_{zz}}{\partial z}, \tag{12}$$

$$\frac{\partial u}{\partial x} + \frac{\partial v}{\partial y} + \frac{\partial w}{\partial z} = 0; \tag{13}$$

$$\tau_{xx} = -u^2 - \overline{u'^2}, \tag{14}$$

$$\tau_{yy} = -v^2 - \overline{v'^2}, \tag{15}$$

$$\tau_{zz} = -w^2 - \overline{w'^2}, \tag{16}$$

$$\tau_{xy} = \tau_{yx} = -uv - \overline{u'v'}, \tag{17}$$

$$\tau_{xz} = \tau_{zx} = -uw - \overline{u'w'}, \tag{18}$$

$$\tau_{yz} = \tau_{zy} = -vw - \overline{v'w'}, \tag{19}$$

where the tildes have been dropped on the understanding that u, v, w (the x, y and z components of $\tilde{\boldsymbol{v}}$) and p are large-scale perturbations defined by (5) and (6). The overbar indicates an ensemble average.

The turbulent spot grows linearly as it travels downstream and the rate of growth is proportional to the spreading half-angle. Hence, the timescale of growth is inversely proportional to the spreading half-angle. Now we define the non-dimensional quantity θ in (3) and subsequent equations to be the spreading half-angle. Carlson *et al.* (1982) estimated that θ is about 0.14 radians (8°). We shall

therefore assume that in the frame of reference moving with the spot, the flow may be considered as quasi-steady and the time derivatives are dropped.

We argue that the variations of the Reynolds stresses are much more rapid in the z-direction than in the other directions, therefore the dominating Reynolds stress terms are $\partial\overline{u'w'}/\partial z$ and $\partial\overline{w'^2}/\partial z$. If we assume that the flow field within the turbulent patch is close to that of the fully developed turbulence in a channel, then the latter term is zero or very small since there is no mean spanwise shear gradient.

Our main interest is in the laminar flow surrounding the turbulent patch. Since large-scale perturbations decay away from the spot, linearization is justified there. Using these assumptions we can, after some algebraic manipulations, simplify the equations to the following form:

$$\frac{1}{Re}\nabla^4 w - U\frac{\partial}{\partial x}(\nabla^2 w) + \frac{\mathrm{d}^2 U}{\mathrm{d}z^2}\frac{\partial w}{\partial x} = -\frac{\partial^3 \overline{u'w'}}{\partial x\,\partial z^2}, \tag{20}$$

$$\nabla^2 p + 2\frac{\mathrm{d}U}{\mathrm{d}z}\frac{\partial w}{\partial x} = -\frac{\partial^2 \overline{u'w'}}{\partial x\,\partial z}, \tag{21}$$

$$\frac{1}{Re}\nabla^2 u - U\frac{\partial u}{\partial x} - \frac{\partial p}{\partial x} - w\frac{dU}{dz} = \frac{\partial \overline{u'w'}}{\partial z}, \tag{22}$$

$$\frac{\partial u}{\partial x} + \frac{\partial v}{\partial y} + \frac{\partial w}{\partial z} = 0, \tag{23}$$

where the operator $\nabla^4 = \nabla^2(\nabla^2)$. Equation (20) is the fundamental equation in the present analysis: a linear non-homogeneous equation with the Reynolds stress term considered as a forcing function. These equations are solved numerically by a combination of Fourier-transform and finite-difference methods with the boundary conditions and the form for the forcing terms discussed below.

The non-slip condition at the walls ($z = \pm 1$) gives

$$u(x, y \pm 1) = v(x, y \pm 1) = w(x, y, \pm 1) = 0. \tag{24}$$

Two more boundary conditions are needed for (20). From (23), since $\partial u/\partial x = \partial v/\partial y = 0$ at the walls, we obtain

$$\frac{\partial w(x, y, \pm 1)}{\partial z} = 0. \tag{25}$$

From (12) we obtain the boundary conditions for the pressure p:

$$\frac{\partial p(x, y, \pm 1)}{\partial z} = \frac{1}{Re}\frac{\partial^2 w(x, y, \pm 1)}{\partial z^2} \tag{26}$$

since all the x- and Y-derivatives vanish at the walls and $\partial\tau_{zz}/\partial z$ has been assumed negligible.

The boundary conditions in the x- and y-directions are that the perturbation quantities should be zero at a distance infinitely far from the disturbance.

Finally, we must assume a form for the function $u'w'$ in order to complete the closure of the problem. Since we are interested only in the solution outside the turbulent region, we assume that the Reynolds stress is a localized disturbance of Gaussian form:

$$\overline{u'w'} = \frac{1}{\epsilon^2} f(z) \exp\left(-\frac{x^2 + y^2}{\epsilon^2}\right), \tag{27}$$

where $f(z)$ is the z-direction distribution of $u'w'$, and ϵ is proportional to the standard deviation of the Gaussian disturbance. As ϵ tends to zero, this function approaches the delta-function. To model finite size of the spot, we distribute this function in an area representing the turbulent spot:

$$\overline{u'w'} = \int\int_S \frac{1}{\epsilon^2} f(z) \exp\left(-\frac{(x-\xi)^2+(y-\eta)^2}{\epsilon^2}\right) \mathrm{d}\xi\, \mathrm{d}\eta, \tag{28}$$

where S is the area taken by the disturbance in the (x, y)-plane.

For the distribution of the concentrated disturbance in the z-direction, we assume a form that allows us to study a general distribution composed of asymmetric and an antisymmetric part:

$$f(z) = c_1(z-z^3)+c_2\cos(\tfrac{1}{2}\pi z), \tag{29}$$

where c_1 and c_2 are constants to allow for asymmetry with respect to z in the input disturbance. Since we are interested in scales of motion larger than the distance between the channel walls, the solution should not be too sensitive to the actual distribution of the forcing across the channel (other than its symmetry). The forcing term enters the problem as the z-derivative of the Reynolds stress $\overline{u'w'}$. Differentiating $f(z)$ with respect to z, we have

$$f'(z) = c_1(1-3z^2)-c_2\tfrac{1}{2}\pi\sin(\tfrac{1}{2}\pi z) \tag{30}$$

where the first and the second terms on the right-hand side give rise to symmetric and antisymmetric forcing respectively. It should be noted that when the forcing is antisymmetric, u and w are antisymmetric and symmetric respectively, and vice versa. The particular choice of the form $f(z)$ is mainly based on simplicity, and in fact, numerical calculations of the structure of the surrounding laminar flow show that, aside from issues of symmetry, different choices of $f(z)$ do not alter the predicted properties.

3. Numerical methods

We use Fourier-transform techniques in x and y combined with a finite-difference method in z to obtain the flow-field solution for a travelling disturbance.

Taking the Fourier transform of u, v, w, p and $\overline{uw}$ with respect to x and y,

$$q(x,y,z) = \frac{1}{4\pi^2}\int_{-\infty}^{\infty}\int_{-\infty}^{\infty} \hat{q}(\alpha,\beta,z)\, \mathrm{e}^{\mathrm{i}(\alpha x+\beta y)}\, \mathrm{d}\alpha\, \mathrm{d}\beta, \tag{31}$$

where q represents any of the variables u, v, w, p and $\overline{u'w'}$, $\hat{q}$ is the Fourier spectrum of q, $\mathrm{i} = \sqrt{-1}$, and α and β are wavenumbers in the x- and y-directions respectively, we obtain the following transformed equations:

$$\left(\frac{\mathrm{d}^2}{\mathrm{d}z_2}-\alpha^2-\beta^2\right)^2\hat{w} - \mathrm{i}\alpha Re\left[U\left(\frac{\mathrm{d}^2}{\mathrm{d}z^2}-\alpha^2-\beta^2\right)-\frac{\mathrm{d}^2U}{\mathrm{d}z^2}\right]\hat{w} = -\mathrm{i}\alpha Re\frac{\mathrm{d}^2\widehat{u'w'}}{\mathrm{d}z^2}, \tag{32}$$

$$\frac{\mathrm{d}^2\hat{p}}{\mathrm{d}z^2}-(\alpha^2+\beta^2)\hat{p} = -2\mathrm{i}\alpha\hat{w}\frac{\mathrm{d}U}{\mathrm{d}z}-\mathrm{i}\alpha\frac{\mathrm{d}\widehat{u'w'}}{\mathrm{d}z}, \tag{33}$$

$$\frac{1}{Re}\left(\frac{\mathrm{d}^2}{\mathrm{d}z^2}-\alpha^2-\beta^2\right)\hat{u}-\mathrm{i}\alpha U\hat{u} = \mathrm{i}\alpha\hat{p}+\hat{w}\frac{\mathrm{d}U}{\mathrm{d}z}+\frac{\mathrm{d}\widehat{u'w'}}{\mathrm{d}z}, \tag{34}$$

$$\mathrm{i}\beta\hat{v} = -\mathrm{i}\alpha\hat{u}-\frac{\mathrm{d}\hat{w}}{\mathrm{d}z}, \tag{35}$$

where (32), the transform of (20), is a non-homogeneous Orr–Sommerfeld equation. The symbol $\hat{}$ is used to denote the spatial transform of the input disturbance.

The transform of a single Gaussian disturbance is

$$\widehat{u'w'} = \pi f(z) \exp\left[\tfrac{1}{4}\epsilon^2(\alpha^2+\beta^2)\right] \tag{36}$$

and the transform of Gaussian disturbances distributed with equal strengths over a finite arbitrary area, S, is

$$\widehat{u'w'} = \pi f(z) \exp\left[\tfrac{1}{4}\epsilon^2(\alpha^2+\beta^2)\right] \iint_S \exp\left[-\mathrm{i}(\alpha\xi+\beta\eta)\right] \mathrm{d}\xi\, \mathrm{d}\eta. \tag{37}$$

In order to evaluate the integral in (37) a finite number of points are chosen on the boundary of S and adjacent points are joined by straight lines. The area S is thus approximated by a polygon. If this polygon is symmetric about $x = 0$, the integral in (37) can be easily evaluated.

The boundary conditions at the walls presented in the last section become

$$\hat{u}(\alpha, \beta, \pm 1) = \hat{v}(\alpha, \beta, \pm 1) = \hat{w}(\alpha, \beta, \pm 1) = 0, \tag{38}$$

$$\frac{\mathrm{d}\hat{w}}{\mathrm{d}z} = 0, \tag{39}$$

$$\frac{\mathrm{d}\hat{p}(\alpha, \beta, \pm 1)}{\mathrm{d}z} = \frac{1}{Re} \frac{\mathrm{d}^2\hat{w}(\alpha, \beta, \pm 1)}{\mathrm{d}z^2}. \tag{40}$$

There are certain symmetry properties which we state below without proof: Conjugate symmetry in α for the same β and z for $\hat{u}$, $\hat{w}$ and $\hat{p}$:

$$\hat{u}(\alpha) = \hat{u}^*(-\alpha), \quad \hat{w}(\alpha) = \hat{w}^*(-\alpha), \quad \hat{p}(\alpha) = \hat{p}^*(-\alpha),$$

where a starred quantity represents its complex conjugate.

Symmetry in β for the same α and z for $\hat{u}$, $\hat{w}$ and $\hat{p}$:

$$\hat{u}(\beta) = \hat{u}(-\beta), \quad \hat{w}(\beta) = \hat{w}(-\beta), \quad \hat{p}(\beta) = \hat{w}(-\beta).$$

Antisymmetry in β for the same α and z for $\hat{v}$:

$$\hat{v}(\beta) = -\hat{v}(-\beta).$$

Conjugate antisymmetry in α for the same β and z for $\hat{v}$:

$$\hat{v}(\alpha) = -\hat{v}^*(-\alpha).$$

With these symmetry properties we only need to calculate a quarter of the Fourier spectrum $(\alpha, \beta, 0)$ to obtain the flow-field solution.

To solve (32), the non-homogeneous Orr–Sommerfeld equation, we apply a higher-order finite-difference scheme based on that devised by Thomas (1953) with 100 spatial steps in the z-direction. The highest derivatives in (33) and (34) are both of second order, which makes possible the direct use of fourth-order central differences to approximate these differential equations.

We obtained $\hat{v}$ from (35) once $\hat{u}$ and $\hat{w}$ are available, except for $\beta = 0$. However, we know that $\hat{v} = 0$ when $\beta = 0$ since $\hat{v}$ is an odd function of β (the antisymmetry property for $\hat{v}$).

Using the fast-Fourier-transform technique for the inverse transform, we sampled the Fourier spectrum at discrete points in the (α, β) – plane using 128 Fourier modes in both x- and y-directions.

4. Numerical results and discussions

Since the frame of reference is fixed to the concentrated disturbance, the basic velocity profile is

$$U(z) = 1 - z^2 - c_s,$$

where c_s is the speed of the concentrated disturbance relative to the laboratory frame.

A general asymmetric distribution of Reynolds stress about the channel centreline can be expressed as the sum of its symmetric and an antisymmetric parts. In the present linear formulation we solve the symmetric and antisymmetric problems separately and the full solution can be obtained by superposition.

4.1. *Effect of changing the speed of the disturbance with antisymmetric forcing*

We use a single Gaussian disturbance and fix $c_1 = 0$ and $c_2 = 0.02$ so that we have an antisymmetric forcing. A series of calculations are carrried out for $0.1 \leqslant c_s \leqslant 0.7$ with the Reynolds number fixed at 1000. Figure 1 shows the w-velocity contours for various values of c_s. The same contour values are used in each plot of figure 1, which range from -0.005 to 0.005. We select, rather arbitrarily, one layer in the channel, i.e. $z = -0.4$, to present our results. The amplitude of the perturbation in the vertical velocity w is largest at the centre of the channel ($z = 0$) and vanishes at the walls ($z = \pm 1$), therefore other choices of z (not too close to the walls) do not alter the basic patterns of the perturbation, but change its amplitude somewhat. In figure 1 and all subsequent figures involving contour plots, the basic flow at $z = 0$ is from left to right. For $c_s = 0.1$, the perturbation to the basic flow is confined to a region close to the origin where the concentrated forcing is located. No apparent wave crests are seen in this case (figure 1*a*). For $c_s = 0.2$, wave crests begin to appear in the contour plots, but extend only a short distance into the surrounding flow (figure 1*b*). For $c_s = 0.25$, wave crests are clearly identifiable and extend farther into the flow (figure 1*c*). As the value of c_s is increased further, more wave crests are seen, their typical wavelengths become shorter. The spread of these wave crests into the surrounding flow reaches a maximum spatial extent at $c_s = 0.4$ approximately, becoming smaller on further increase of c_s. The typical wavelengths become shorter and the angles of the wave crests increase. At $c_s = 0.7$, the perturbation to the basic flow shrinks to the vicinity of the concentrated forcing (figure 1*d*, *e*, *f*).

These results are related to the Orr–Sommerfeld eigenvalue problem. Figure 2(*a*, *b*) shows the temporal eigenvalues of Poiseuille flow at $Re = 1000$. The real part, c_r, and imaginary part, c_i, of the eigenvalue, c, are plotted against the absolute wavenumber, $k = (\alpha^2 + \beta^2)^{\frac{1}{2}}$, for various fixed β. The least stable mode occurs at approximately $k = 1.35$ and $c_r = 0.4$. Since the spot speed c_s is real we do not have an exact resonance with the free Tollmien–Schlichting waves which have no real eigenvalue c at $Re = 1000$. However, the least stable Tollmien–Schlichting mode has a small imaginary part, c_i (≈ -0.03 in this case); near-resonance is expected when $c_s = c_r$. This explains why the most effective spreading of the wave crests occurs when the speed of the concentrated disturbance c_s is 0.4.

It is important to note several facts concerning experimental observations. In the flow visualization study of Carlson *et al.* (1982), the front and the rear of the turbulent spot travel with speeds of approximately 0.67 and 0.33 respectively. The phase speed of the wave crests in this experiment was estimated by Widnall (1984) to be approximately 0.4 at $Re = 1000$. This agrees very well with our calculations in that the phase speed is very close to that of the least stable Tollmien–Schlichting

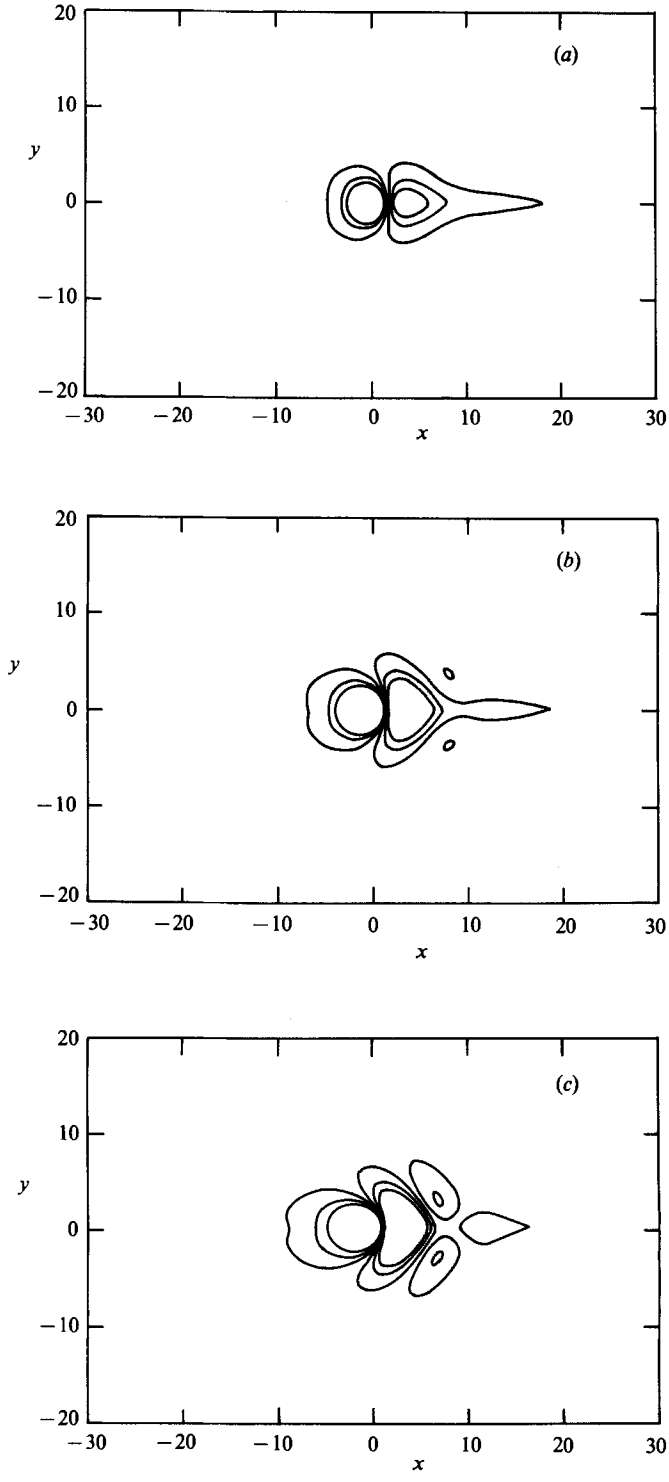

FIGURE 1 (*a–c*). For caption see next page.

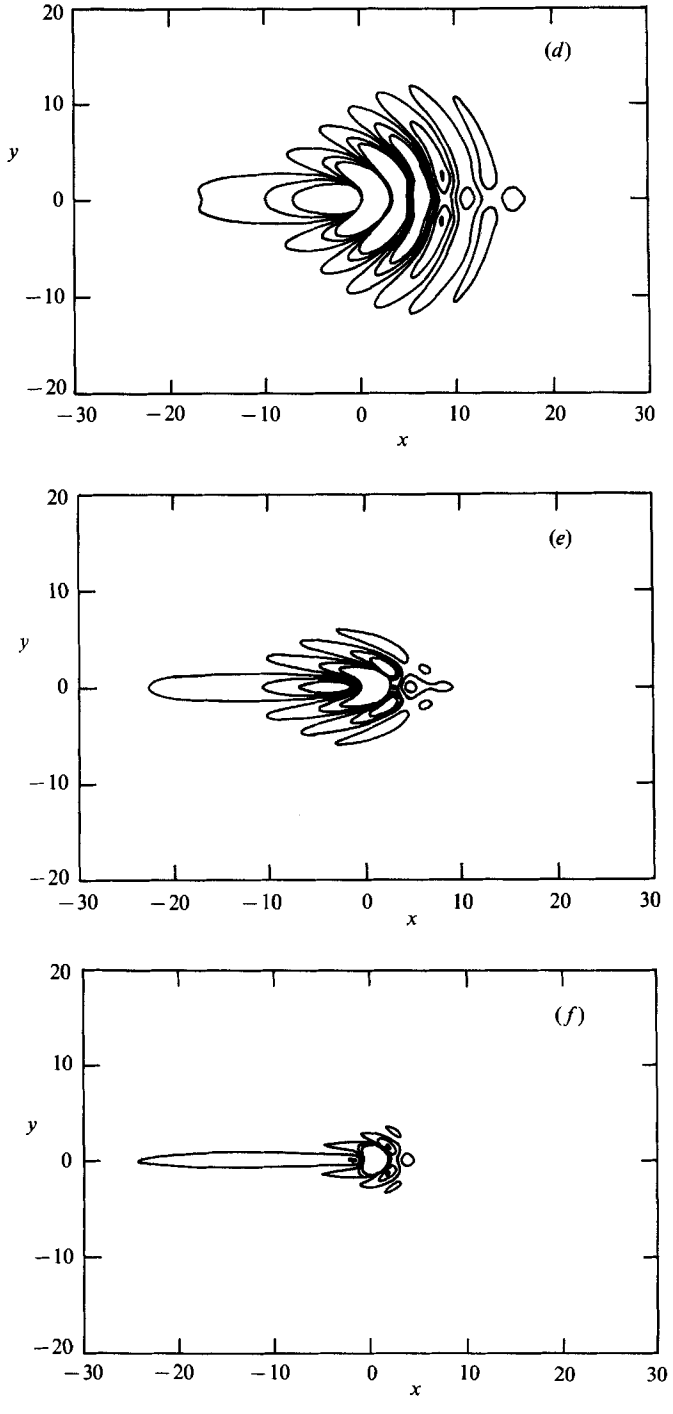

FIGURE 1. Contour plots of velocity component w for $Re = 1000$, $z = -0.4$, $c_1 = 0$ and $c_2 = 0.02$. Contour values range from -0.005 to 0.005, increment $= 0.002$. (*a*) $c_s = 0.1$, (*b*) 0.2, (*c*) 0.25, (*d*) 0.4, (*e*) 0.55, (*f*) 0.7.

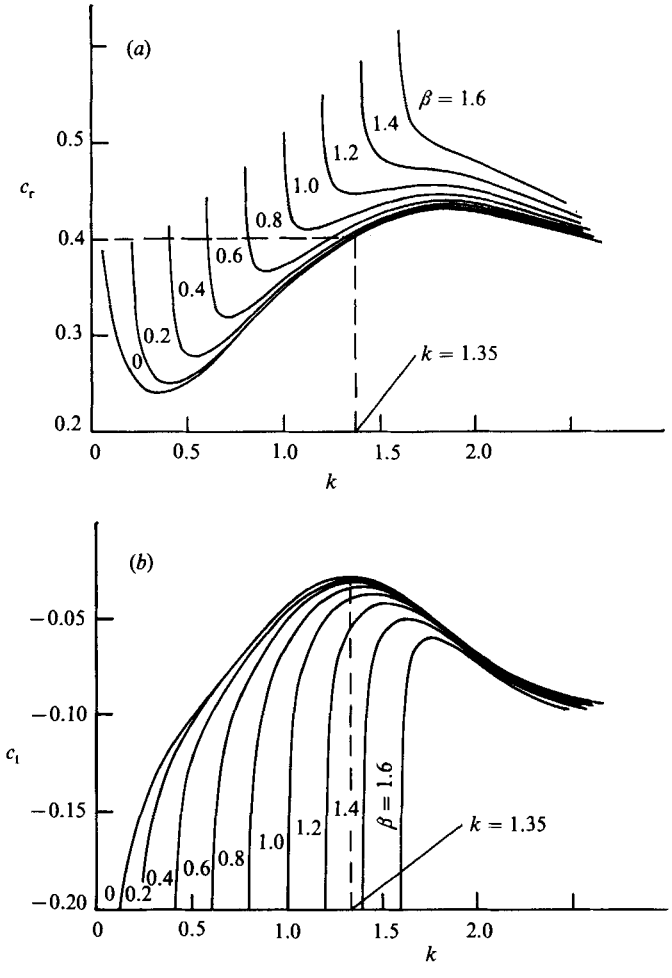

FIGURE 2. Temporal eigenvalues, $c(\alpha,\beta) = c_r(\alpha,\beta) + ic_i(\alpha,\beta)$, of plane Poiseuille flow at $Re = 1000$. (*a*) c_r *vs.* k for various β. (*b*) c_i *vs.* k for various β, where $k = (\alpha^2+\beta^2)^{\frac{1}{2}}$.

mode. However, the flow visualization experiment of Alavyoon *et al.* (1986) showed that 'no turbulent spots could be generated no matter how large the (initial injecting-jet) disturbance was' for $Re < 1100$. The front and the rear of their spot travel at higher speeds (≈ 0.75 and 0.62 respectively) than those measured by Carlson *et al.* (1982). The full Navier–Stokes simulation of Henningson *et al.* (1987) performed at $Re = 1500$ seems to confirm the observations of Alavyoon *et al.* (1986). In both Alavyoon *et al.* (1986) and Henningson *et al.* (1987) the spots shown were well-developed ones at distances of over 100 channel half-depths downstream of the triggering position, whereas, Carlson *et al.* (1982) showed photographs of spots in the early stages of development, i.e. at distances of about 50 channel half-depths downstream of the trigger, showing wave patterns quite different from those in figure 3 of Henningson *et al.* (1987), but more like the results shown in figure 1 of the present paper. It may be that the early stages of the spot development is different from that in the later stages. Further experiments and simulations have to be done before these questions can be answered. Our model may provide information about the early stages of the spot development where the wave field around the spot resembles that

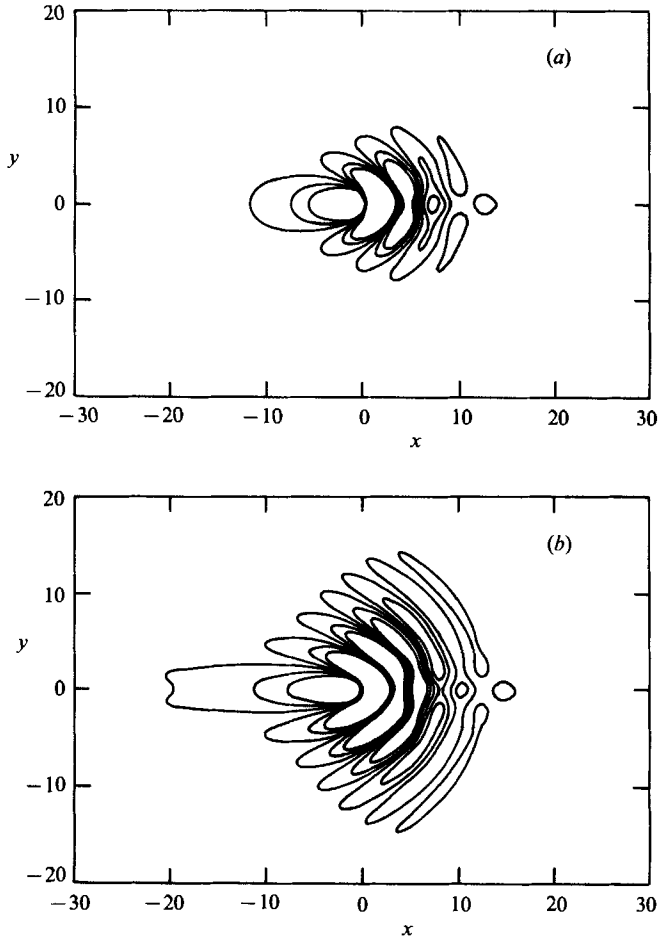

FIGURE 3. Contour plots of the velocity component w, $c_s = 0.4$ and $z = -0.4$ with $c_1 = 0$, $c^2 = 0.02$. (*a*) $Re = 500$, (*b*) 1500. (See figure 1*d* for $Re = 1000$). Contours have the same values as in figure 1.

of Carlson *et al.* (1982). In any case, we do not expect a linear calculation to give a complete model for the development of the turbulent spot.

4.2. *Effect of Reynolds number with antisymmetric forcing*

Here, we are interested in the effect of changing the Reynolds number on the wave field generated by the concentrated disturbance of the form (27) with antisymmetric forcing. We assume that the disturbance is travelling with speed $c_s = 0.4$ in the laboratory frame. We repeated the calculations at three different Reynolds numbers, $Re = 500$, 1000 and 5000.

Figure 3 shows the contour plot of the w-velocity for one layer in the channel, $z = -0.4$. We can see wave crests becoming more and more oblique as they extend into the surroundings. At $Re = 500$, the wave crests are heavily damped spatially. As the Reynolds number is increased the wave crests radiate out into the surroundings whereas the wavelengths and the oblique angles hardly change at corresponding positions in the flow. In the flow visualization study of Alavyoon *et al.* (1986) and experiment of Henningson & Alfresson (1987) the spreading half-angle of the turbulent spot was found to increase with the Reynolds number. The results of our

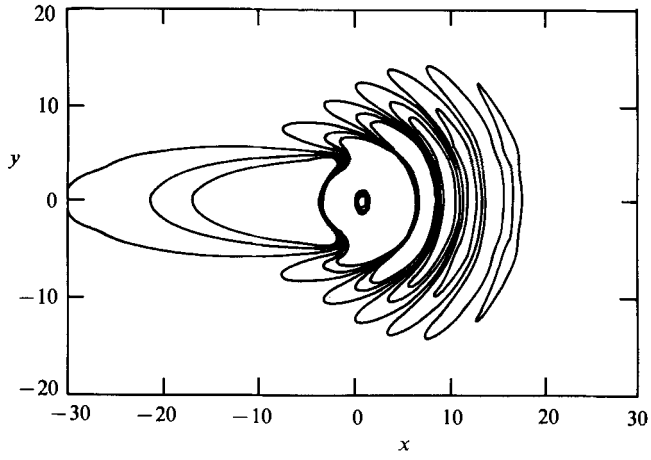

FIGURE 4. Contour plot of w for $Re = 1000$, $c_s = 0.4$ and $z = -0.4$ with disturbances distributed in a circle of diameter 10 centred at $(0, 0)$. $c_1 = 0$, $c_2 = 0.02$. Contours plotted have the same values as in figure 1.

calculations are consistent with their experiments. The wavelength of a typical wave around the concentrated disturbance was measured from figure 3 to be approximately 5.0, and showed no appreciable change over the Reynolds number range 500 to 1500. In their experiment, Henningson & Alfredsson (1987) found that the dominant wavelength was 4.6 at $Re = 1500$. (We also calculated flow patterns for various values of c_s at $Re = 1500$. The greatest extent of flow disturbance occurred at about $c_s = 0.4$. Only these results are presented.)

4.3. *Effect of the scale of the concentrated disturbance with antisymmetric forcing*

In §§4.1 and 4.2 we presented results for a disturbance of very small spatial extent. The available experimental results, e.g. Carlson *et al.* (1982), show that the typical scale of a turbulent spot is about 10 to 20 times the channel half-depth. It is natural to ask whether the properties of the wave crests generated by the region of turbulence depend on the scale of this region. We model the spatial scale of the turbulent spot by distributing the Gaussian disturbance over a finite area, S (see (37)).

Equation (37) can be integrated analytically if the region S is approximated by an n-sided polygon symmetric about the x-axis and with the jth side described by $\eta = k_j \xi + r_j$, where (ξ, η) is a point on the jth side and k_j and r_j are, respectively, the slope and the intersection point with the y-axis if the jth side were extended. We have

$$\iint_S \exp\left[-\mathrm{i}(\alpha\xi+\beta\eta)\right] \mathrm{d}\xi\, \mathrm{d}\eta = \sum_j \left[\frac{\mathrm{e}^{-\mathrm{i}((\alpha-k_j\beta)\xi_{j+1}-\beta r_j)} - \mathrm{e}^{-\mathrm{i}((\alpha-k_j\beta)\xi_j-\beta r_j)}}{(\alpha-k_j\beta)\beta} - \frac{\mathrm{e}^{-\mathrm{i}((\alpha+k_j\beta)\xi_{j+1}+\beta r_j)} - \mathrm{e}^{-\mathrm{i}((\alpha+k_j\beta)\xi_j+\beta r_j)}}{(\alpha+k_j\beta)\beta} \right], \quad (41)$$

where the ξ_j are the streamwise coordinates of the corners of the polygon. The above expression is continuous in α and β everywhere, since the integrand is continuous. At $\alpha/\beta = \pm k_j$ and $\beta = 0$, the values of the terms in the summation are defined by their limits as $\alpha/\beta \to \pm k_j$ and $\beta \to 0$.

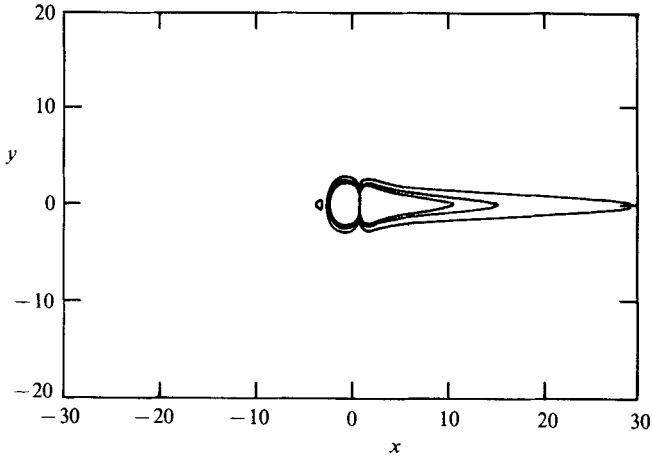

FIGURE 5. Contour plot of w. $Re = 1000$, $c_s = 0.4$, $z = -0.4$, $c_1 = 0.1$ and $c_2 = 0$. Contours plotted have the same values as in figure 1.

We take the region S to be a circle of diameter 10 and approximate it by a 16-sided polygon. Contours of constant w for the flow field due to this extended disturbance are shown in figure 4. The typical wavelength of the disturbance measured from figure 4 is approximately 5.0 for $Re = 1000$, unchanged from the value for a single Gaussian disturbance (figure 1). Calculations were also carried out for different parameters c_s and Re; the typical wavelength in each case is the same as that obtained in the single-disturbance case at corresponding c_s and Re. The wavelength appears to be insensitive to the spatial extent of the disturbance. Therefore, the results of calculations using a single Gaussian disturbance are sufficient to represent the essential features of the wave field around a large disturbance.

4.4. *Numerical results with symmetric forcing*

We use a single Gaussian disturbance symmetric with respect to the channel centreline and take $c_1 = 0.1$, $c^2 = 0$, $c^s = 0.4$ and $Re = 1000$. The contour plot of the vertical velocity w is shown in figure 5 ($z = -0.4$). The perturbation to the basic flow is confined to the vicinity of $x = 0$ with an arrow-shaped region leading the concentrated disturbance. We do not observe any identifiable wave crests such as those we see in figure 1 associated with antisymmetric forcing. Calculations with different parameter values Re and c_s show similar patterns of perturbation. As c_s increases the 'arrow head' leading the concentrated disturbance becomes increasingly shorter and an 'arrow tail' of similar shape begins to trail the disturbance. At about $c_s = 0.8$ the 'head' disappears almost completely leaving only the long 'tail' trailing the disturbance.

Figure 12 of Henningson & Alfredsson (1987) shows the measured spanwise velocity profiles in the region where the waves are seen. In front of the spot the flow direction is towards the spot centreline. When about half of the spot (or what they termed the 'wingtip') has passed, the flow close to the wall remains towards the centreline whereas the flow near the centre of the channel is away from the centreline. Their profiles were measured at different instants in time at a fixed station in space as the spot travelled.

Since their experimental results discussed above show spanwise velocity profiles

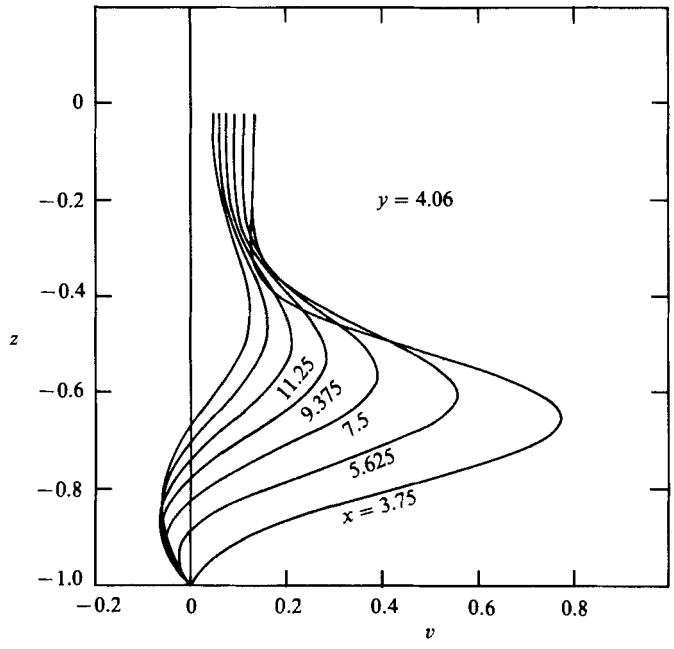

FIGURE 6. Spanwise velocity profiles at different streamwise stations at a fixed spanwise position. The centre of the spot is at $x = 0$ and $y = 0$. $Re = 1500$.

around the spot, we present our numerical results in figure 6 for the spanwise velocity profile over half of the channel at some selected streamwise stations for a fixed spanwise station on one side of the disturbance. The spanwise velocity close to the wall is towards the spot centreline, and is away from the centreline far from the wall, indicating the presence of streamwise vorticity. This is a result of the pressure gradient associated with the curvature of streamlines around the disturbance. Figure 6 shows similarities to figure 12 of Henningson & Alfredsson (1987). Here, we do not attempt to compare our linear calculations with the experiment quantitatively since the process by which the velocity profile is distorted is a highly nonlinear one. Figure 6 merely shows the tendency of a symmetric disturbance to create an inflectional velocity profile, and hence change the stability properties of the basic flow.

In the experiment of Henningson & Alfredsson (1987) the u-perturbation field around the turbulent spot was found to consist of waves antisymmetric (in u) with respect to the channel centreline and, earlier, the experiment of Nishioka *et al.* (1975) also showed that the two-dimensional linear waves in plane Poiseuille flow are antisymmetric (in u). According to linear theory the least-damped waves are antisymmetric, and the symmetric waves are strongly damped. It is, therefore, not surprising that we do not see identifiable wave crests with symmetric forcing in the present simple linear model. The moving disturbance merely distorts the basic velocity profile, modifying the basic flow and its stability properties. Nonlinear analysis is required to study the change of the wave field due to the change in basic flow.

4.5. *Perturbation amplitude and forcing strength*

In our formulation the velocity perturbations are proportional to the strength of the Reynolds-stress forcing terms. The strengths of the concentrated disturbances c_1 and

c_2 (see (30)) represent the magnitude of the Reynolds stress integrated over the area on which it acts. The ratio of the linear perturbation amplitudes to forcing strength is a measure of the effectiveness of the concentrated disturbance.

We can use estimates of the strength of the forcing to determine the magnitude of the velocity perturbations for comparison with the experimental data of Henningson & Alfredsson (1987). For $Re = 1500$, in the plane $z = 0.6$ at a spanwise distance of four times the channel half-depth (conditions chosen for comparison with experimental data) we found that the maximum amplitude of the u-velocity ratio to the strength of the forcing was $u/c_1 \approx 1$ and $u/c_2 \approx 4$ for symmetric and antisymmetric disturbances respectively. Since experimental data are unavailable for $Re = 1500$ we use the data of Eckleman (1974) at $Re = 2800$ to estimate the magnitude of the Reynolds stress. From these data we deduced that the maximum value of $\partial u'w'/\partial z$ is approximately 0.022. From experiments we estimate the area of a turbulent region to be about 20 times the square of the channel half-depth. Thus the strength of the forcing over the spot area is 0.44. Our model for the region of turbulence is a Gaussian function with an integrated area of π. If we relate our model to the experimental data at the same maximum value of $\partial u'w'/\partial z$, we obtain an estimate for c_1 of about 0.09 from (27) and (30). This strength of symmetric forcing would produce a symmetric u-velocity perturbation of about 10%.

On the other hand, we could use the measured amplitudes of the antisymmetric disturbance (Henningson & Alfredsson) to estimate the magnitude of antisymmetric forcing. This would give a value for c_2 of about 0.01. We can then ask what ratio of symmetric to antisymmetric forcing would be required to produce the observed wave amplitude of about 0.04. Our model predicts that an asymmetry in Reynolds stress of about 10% is required to produce the observed wave amplitude.

Thus the predictions of the linear model are in reasonable agreement with the observed perturbation velocities for symmetric disturbances for which a direct estimate can be made. The estimate of asymmetric disturbances can only be inferred since the asymmetry of the quasi-steady Reynolds stress forcing is not known. However, the flow is found to be particularly sensitive to antisymmetric forcing.

5. Conclusion

Using linear theory to present flow patterns created by a steady travelling concentrated disturbance of Reynolds stress in plane Poiseuille flow, provides some insight into the observed structure around a turbulent spot. The region of small-scale turbulence was modelled by a concentrated distribution of Reynolds stress or a distribution of such disturbances over a finite area when the effect of finite spatial extent was considered. In general this forcing term can be regarded as the sum of a symmetric function and an antisymmetric function. The following conclusions can be drawn from numerical calculations using this model.

Antisymmetric forcing produces a spatially damped wave packet around the disturbance at Reynolds numbers below the critical value of linear theory. These waves become less damped spatially as the Reynolds number increases; this may be related in some way to the increase with Reynolds number of spreading half-angle of the spot observed in some experiments. The typical wavelength measured from the contour plots of the cross-channel velocities is approximately 5.0 for Reynolds numbers from 500 to 2000 and for a disturbance travelling with speed $c_s = 0.4$; this wavelength is close to that observed by Henningson & Alfredsson (1987) (approximately 4.6 at $Re = 1500$). The typical wavelength is insensitive to the scale

of the region of disturbance that creates the waves. The shape of the wave packet and wave sweep-back angles in the contour plots of the calculated cross-channel velocity are in qualitative agreement with those in photographs taken by Carlson *et al.* (1982). Increasing the speed c_s of the disturbance from 0.1 to 0.7 produces, at first, a less spatially damped wave field with decreasing wavelength. Spatial damping reaches a minimum at about $c_s = 0.4$. As c_s is increased further, the extension of the wave crests into the surrounding flow becomes less effective and the disturbance is confined to the immediate vicinity of the steady forcing disturbance. Only small asymmetry in Reynolds stress is required to create the observed wave amplitudes.

Symmetric forcing does not produce an identifiable wave field, but is found to distort the basic velocity profile – the blockage effect. The picture we present is not inconsistent with, but rather complementary to, the work of Henningson & Alfredsson (1987) and Henningson *et al.* (1987). In their work they pointed out that the symmetric blockage effects modify the velocity profile to slightly destabilize the antisymmetric waves. In our work we show that antisymmetric forcing generates antisymmetric waves while blockage modifies the velocity profile. In a fully nonlinear formulation of the problem both these mechanisms would contribute to the observed wave field. The nonlinear interactions between the symmetric and antisymmetric modes required for a complete description of the flow field are beyond the scope of the present linear analysis, and are left to future studies.

This research was supported by National Science Foundation under Grant MSM-8211478.

REFERENCES

ALAVYOON, F., HENNINGSON, D. S. & ALFREDSSON, H. 1986 Turbulent spots in plane Poiseuille flow – flow visualization. *Phys. Fluids* **29**, 1328.

CARLSON, D. R., WIDNALL, S. E. & PEETERS, M. F. 1982 A Flow-visualization study of turbulent spots in plane Poiseuille flow. *J. Fluid Mech.* **121**, 487.

ECKELMANN, H. 1974 The structure of the viscous sublayer and the adjacent wall region in a turbulent channel flow. *J. Fluid Mech.* **65**, 439.

GASTER, M. 1975 A theoretical model of a wave packet in the boundary layer on a flat plate. *Proc. R. Soc. Lond.* A **347**, 371.

GASTER, M. & GRANT, I. 1975 An experimental investigation of the formation and development of a wave packet in a laminar boundary layer. *Proc. R. Soc. Lond.* A **347**, 253.

HENNINGSON, D. S. & ALFREDSSON, H. 1987 The wave structure of turbulent spots in plane Poiseuille flow. *J. Fluid Mech.* **178**, 405.

HENNINGSON, D. S., SPALART, P. R. & KIM, J. 1987 Numerical simulations of turbulent spot in plane Poiseuille and boundary-layer flow. *Phys. Fluids* **30**, 2914.

LANDAHL, M. T. 1975 Wave breakdown and turbulence. *SIAM J. Appl. Maths* **28**, 735.

NISHIOKA, M., IIDA, S. & ICHIKAWA, Y. 1975 An experimental investigation of the stability of plane Poiseuille flow. *J. Fluid Mech.* **72**, 731.

ORSZAG, S. A. 1971 Accurate solution of the Orr–Sommerfeld stability equation. *J. Fluid Mech.* **50**, 689.

ORSZAG, S. A. & KELLS, L. C. 1978 Transition to turbulence in plane Poiseuille and plane Couette flow. *J. Fluid Mech.* **96**, 159.

ORSZAG, S. A. & PATERA, A. T. 1980 Subcritical transition to turbulence in plane channel flows. *Phys. Rev. Lett.* **47**, 989.

ORSZAG, S. A. & PATERA, A. T. 1981 Subcritical transition to turbulence in planar shear flows. In *Transition and Turbulence* (ed. R. E. Meyer), p. 127. Academic.

ORSZAG, S. A. & PATERA, A. T. 1983 Secondary instabilities of wall bounded shear flows. *J. Fluid Mech.* **128**, 347.

REYNOLDS, O. 1883 An experimental investigation of the circumstances which determine whether the motion of water shall be direct or sinuous, and of the law of resistance in parallel channel. *Phil. Trans. R. Soc. Lond.* **174**, 935.

STUART, J. T. 1960 On the non-linear mechanics of wave disturbances in stable and unstable parallel flows. Part 1. The basic behaviour in plane Poiseuille flow. *J. Fluid Mech.* **9**, 353.

THOMAS, L. H. 1953 The stability of plane Poiseuille flow. *Phys. Rev.* **91**, 780.

WIDNALL, S. E. 1984 Growth of turbulent spot in plane Poiseuille flow. In *Turbulence and Chaotic Phenomena in Fluids* (ed. T. Tatsumi) p. 93. Elsevier.